GaSb homojunctions for far-infrared (terahertz) detection

P. V. V. Jayaweera, S. G. Matsik, and A. G. U. Perera[a)]
Department of physics and Astronomy, Georgia State University, Atlanta, Georgia 30303

Y. Paltiel, Ariel Sher, and Arie Raizman
Solid State Physics Group, Soreq NRC, Yavne 81800, Israel

H. Luo and H. C. Liu
Institute for Microstructural Sciences, National Research Council, Ottawa K1A 0R6, Canada

(Received 5 December 2006; accepted 9 February 2007; published online 14 March 2007)

A GaSb based homojunction interfacial work function internal photoemission far-infrared (>30 μm) detector is presented. Metal-organic vapor phase epitaxy grown *p*-GaSb/GaSb samples show 9.7 A/W peak responsivity and a peak detectivity of 5.7×10^{11} Jones with effective quantum efficiency of 33% at 36 μm and 4.9 K. The detector exhibits a 97 μm (~3 THz) free carrier response threshold wavelength. Results indicate that *p*-GaSb homojunction internal work function internal photoemission detectors are promising candidates to be a competitor for terahertz applications. © *2007 American Institute of Physics*. [DOI: 10.1063/1.2713760]

Much of the recent interest in terahertz frequency between 10 to 0.3 THz (30 μm and 1 mm) radiation stems from the ability to penetrate many organic materials without the ionizing damage associated with short wavelength radiation such as x rays.[1] Another important feature is the fact that terahertz radiation is readily absorbed by water. This allows terahertz radiation to distinguish between materials with varying water content, for example, fat versus lean meat. These properties offer various applications related to process and quality control, as well as biomedical imaging.[2] Moreover, tests are currently under way to determine whether terahertz tomographic imaging can augment or replace standard mammography. Others have proposed terahertz imaging as a method of screening passengers for explosives at airports. For military and astrophysics uses, terahertz detectors have many applications such as early detection of long range missiles, concealed weapon identification, and space based astronomy. Those studies explain the reasons for the surging demand of high performance terahertz detectors in recent years.

Charge transport properties[3] and terahertz absorption[4] of high quality GaSb films were reported elsewhere. Infrared (IR) detectors based on type II InAs/GaSb superlattices[5] have been demonstrated for the 3–5 μm (Ref. 6) and 8–12 μm (Ref. 7) transparency bands of the atmosphere. The longest zero response threshold wavelength reported was 20 μm.[8] This letter reports the results for a GaSb based homojunction interfacial work function internal photoemission (HIWIP) detector. The active region of a HIWIP detector consists of one or more periods, each consisting of a series of doped emitter and undoped barrier layers. In HIWIP detectors, the incident photons are absorbed in the emitter layers by the free carrier absorption mechanism, and under suitable bias conditions the photoexcited carriers with energy $h\nu$ larger than the band-edge offset between the doped emitter layer and the undoped barrier region are emitted across the junction and then collected. For a homojunction, the band offset is determined by the doping-induced band gap narrowing of the emitter.[9] The internal photoemission of the carriers is characterized by the interfacial work function Δ, which corresponds to the energy difference between the bottom of the barrier (for a *p*-HIWIP) and the Fermi level in the emitter. In general, these detectors show broad band response due to free carrier absorption which involves initial and final energy states within the same continuum. The zero response threshold frequency f_0 is introduced only in the photoemission stage. Therefore, the threshold frequency of the detector $f_0=0.242\Delta$ with f_0 in terahertz and Δ in meV or the zero response threshold wavelength of the detector $\lambda_0=1240/\Delta$, where λ_0 in micrometer and Δ in meV.

The HIWIP structure was grown on GaSb substrates at a temperature of 600 °C and a reactor pressure of 400 Torr by metal-organic vapor phase epitaxy[10] using a Thomas Swan vertical reactor. Conventional trimethylgallium and trimethylantimony were used as precursors. The structure of the detector grown on a 0.7 mm thick 5×10^{18} cm^{-3} *p*-doped GaSb substrate, consisted of a 0.05 μm thick 2×10^{18} cm^{-3} *p*-doped bottom emitter, a 2 μm thick undoped barrier, a 0.05 μm thick 2×10^{18} cm^{-3} *p*-doped top emitter, and a 0.1 μm thick 5×10^{18} cm^{-3} *p*-doped top contact. Zinc was the dopant with diethylzinc used as the dopant source. The detector was fabricated by etching different size mesas using wet etching techniques. Ti/Pt/Au Ohmic contacts were evaporated for both the top and bottom contacts. Figure 1 shows a schematic view of the detector and its relevant band diagram after the device processing.

Dark and 300 K background current voltage (*IV*) characteristics of the sample were measured at various temperatures using a Keithley 2400 source meter with the sample mounted on the cold finger of a close cycle refrigerator. The spectral response measurements were carried out using a Perkin-Elmer System2000 Fourier-transform infrared (FTIR) spectrometer with a Si composite bolometer as the reference. The sample was mounted in a liquid He Dewar made by Infra-Red Laboratory Inc. The same setup was connected to a SR-785 two-channel fast Fourier-transform signal analyzer coupled to a SR-560 high impedance low-noise voltage preamplifier for noise current density measurements.

The sample GSU-A3 contains square mesas with sides of 400, 600, 800, and 1000 μm. Figure 2 shows the mea-

[a)]Electronic mail: uperera@gsu.edu

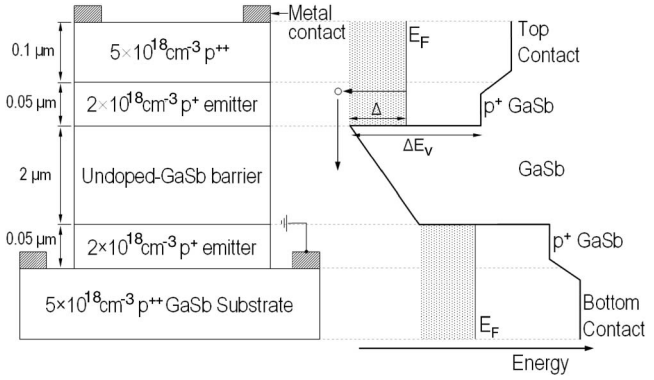

FIG. 1. Schematic drawing of the processed detector on the left and an energy-band diagram with the detection mechanism of the device under forward bias on the right. The internal work function Δ originates from the doping offset between the emitter and the barrier. Here ΔE_V is the valence-band-edge offset at the p^+ and undoped interface, E_F the Fermi level relative to the valence-band edge.

sured dark current density variation with bias voltage for eight different mesas of the sample at 10 K. Current densities are almost the same for different size mesas of untreated samples, showing that it is free of major sidewall/surface leakage. Normally larger devices (400–1000 μm) are not affected very much by surface leakage, which often occurs for devices less than about 50×50 μm^2. The dark current density for an 800 μm mesa at 4.9 K is also shown in Fig. 2. The measured responsivity of GSU-A3 under different bias voltages in the range of 20–44 μm is shown in Fig. 3(a). An increase in responsivity can be observed for applied bias increasing up to a field of 18.5 kV/cm (3.7 V), above this field the responsivity started to saturate. The maximum response, 9.7 A/W, was obtained at 36 μm under 3.7 V bias. The detector shows a maximum detectivity of 5.7×10^{11} Jones at 3 V bias. Above this voltage, the noise current is higher due to the low dynamic resistance of the sample, reducing the

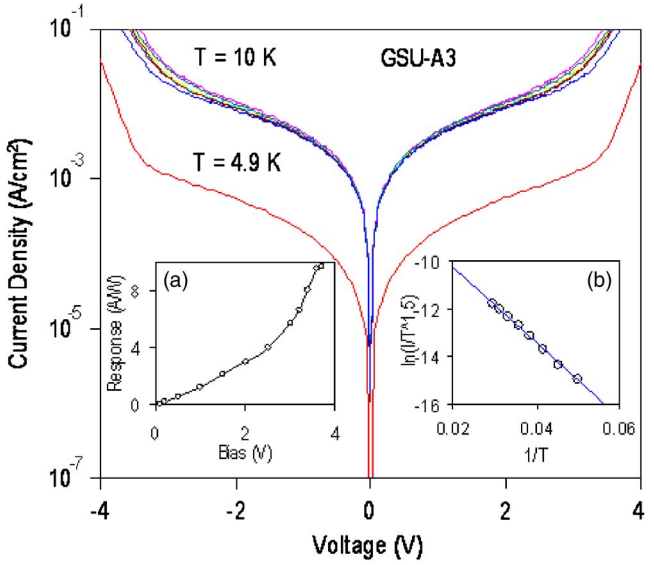

FIG. 2. (Color online) Dark current density vs bias voltage for eight different mesas in sample GSU-A3 measured at 10 K shows good uniformity of the structure. A single dark *IV* curve for one mesa at the 4.9 K spectral measurement temperature is also shown. Inset (a) shows an Arrhenius curve from which a Δ of 12.8±0.3 meV is calculated. Inset (b) shows the bias dependence of the peak responsivity at 4.9 K. The responsivity was almost linear (with a slope of 1.6 A/W V) for low biases (<2.5 V).

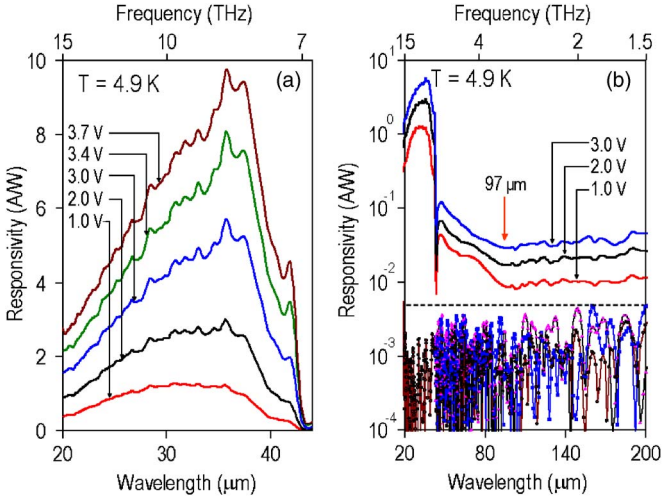

FIG. 3. (Color online) Spectral response as measured at 4.9 K for sample GSU-A3 under different forward bias voltages. (a) The 20–43 μm range responsivity with peak responsivity of 9.7 A/W at 36 μm and 3.7 V bias. (b) The full spectrum including the long wavelength responses at 1, 2, and 3 V bias conditions. Note that the response is plotted in a log scale in order to emphasize the long wavelength response. The arrow shows the 97 μm free carrier response threshold wavelength position. The noise curves at the bottom were taken by blocking the FTIR source beam, and the dashed line shows the maximum noise level of the spectral response measurement setup.

detectivity at 3.7 V bias. Responsivity decreases with increasing operating temperature and no significant signal could be measured above 15 K. The responsivity drops to zero around 43 μm due to the reststrahlen band of GaSb. Figure 3(b) shows the full responsivity range from 20 to 200 μm for 1, 2, and 3 V biases, with the corresponding background noise level [in the bottom of Fig. 3(b)] was measured after blocking the IR beam of the FTIR spectrometer by using a thick metal plate, and the corresponding response curve is the noise level. Above the reststrahlen absorption minimum at 43 μm, the response initially increases and then gradually decays up to the 97 μm threshold. At lower frequencies (longer wavelengths), the sample shows a clear but low flat response up to 1.5 THz (200 μm). This response is relatively low compared with the peak response at 8.3 THz (36 μm) but clearly an order of magnitude above the noise level. The 20–43 μm photoresponse does not exhibit any dependence on measurement speed (optical path difference velocity of FTIR); however, the constant long wavelength tail (43–200 μm) response increases with decreasing measurement speed. A second sample processed in a different laboratory displayed a similar flat response long wavelength tail, confirming that it is not processing or contact related. The zero response threshold wavelength λ_0 of the detector is not clearly visible, since it corresponds to two different overlapping response mechanisms. The free carrier threshold of $\lambda_0=97$ μm [arrow in Fig. 3(b)] was obtained by selecting the intersection point of the flat long wavelength response with the free carrier response. This value agrees well with calculated Arrhenius Δ value. The inset (b) of Fig. 2 shows the $\ln(I/T^{1.5})$ vs I/T plot that was used to calculate the internal work function Δ. The long wavelength flat response mechanism is not yet clearly understood.

The response time of the detector can be estimated from the bias dependent responsivity measurements.[11,12] For low experimental temperatures ($T\sim4.2$ K), the current responsivity R at a bias voltage V can be expressed as

$$R = \frac{3q\eta\mu\tau}{2d^2}\frac{1}{k_B T_0}V, \tag{1}$$

where q is elementary charge, η is the absorption quantum efficiency, μ the mobility, k_B is the Boltzmann constant, d the detector thickness, T_0 is the equilibrium temperature, and τ is the energy relaxation time of the hot carriers. The energy relaxation time could give the lower limit for the detector response time and could be regarded as the response time for an ideal detector. Inset (a) of Fig. 2 shows the bias dependence of the responsivity measured at 4.9 K. At low voltages ($V<2.5$ V) the responsivity increases linearly with bias. For both intrinsic and extrinsic photoconductive detectors at a given bias, the responsivity is proportional to the response time. Absorption quantum efficiency η can be expressed as described in Ref. 11,

$$\eta = \frac{1-e^{2\alpha l}}{e^{(d/L_Z)}}. \tag{2}$$

Here α, l, and L_z are the absorption coefficient, thickness of the emitter layer, and inelastic scattering mean free path, respectively. Using the GaSb α from Ref. 4 and taking L_z as 1 μm, the total absorption quantum efficiency was calculated as 17.3%. Using detector thickness d of 2.1 μm, the measured mobility[4] of 200 cm^2/V s for similar doping levels, and the slope of 1.6 A/W V measured from the linear region (0–2.5 V) of R vs V plot, the response time of the detector is estimated to be of the order of a few picoseconds. The photocurrent gain values g are calculated for the peak response (36 μm) as 0.6 at 2 V and 1.9 at 3.7 V biases from the combination of $R=q\eta g\lambda/hc$ with Eq. (2), where h, c, and λ are the Planck constant, speed of light, and wavelength at peak response. The effective quantum efficiencies ηg were calculated as 10 and 33 for 2 and 3.7 V biases, respectively. The above photocurrent gain numbers and calculated shot noise gain[13] numbers differ for this sample. This difference and the unusually high impedance of the sample are believed to be due to the Schottky-type contacts.[14] Further studies are needed to examine the effects of Schottky contact on HIWIP detectors.

In conclusion, GaSb based HIWIP detectors with 97 μm (~3 THz) zero response threshold wavelength were demonstrated. The detectors have a peak responsivity of 9.7 A/W and peak detectivity of 5.7×10^{11} Jones at 4.9 K. In this study a simple single emitter/barrier structure was utilized showing high response. The response could be enhanced even further by using multilayer structures which will increase the photon absorption efficiency and could possibly induce photocurrent gain enhancment.[15] The doping offset of the emitter and barrier determined the threshold of the HIWIP detector. Using heterojunction interfacial work function internal photoemission (HEIWIP) structures[13] such as $In_xGa_{1-x}Sb/GaSb$ would give a flexible system to control the threshold. Estimations show that, with the variation of the In fraction, 1 THz (300 μm) threshold could be achieved while keeping the accuracy of the In fraction in the practical range (a variation of 2.5% will only change the work function by 1 meV). One of the major problems in achieving a 1 THz threshold with GaAs/AlGaAs or GaN/AlGaN system is the need for very high Al fraction accuracies (0.2% for AlGaAs and 0.05% for AlGaN) that is on or beyond the edge of the experimental capabilities. Therefore GaSb/InGaSb is a promising material for terahertz detection. Resonant cavity enhanced GaAs/AlGaAs HEIWIP's have already been demonstrated,[16] and resonant cavities can be easily incorporated into GaSb based detectors to further enhance the response.

This work was supported in part by the U.S. NSF under Grant Nos. ECS 05-53051, INT-0322355 and OISE 054325. The Soreq NRC group would like to thank the outstanding technical support of Shmuel Saad for the metal-organic chemical vapor deposition maintenance and Galit Shturm for the fabrication process.

[1] S. W. Smye, J. M. Chamberlain, A. J. Fitzgerald, and E. Berry, Phys. Med. Biol. **46**, R101 (2001).
[2] P. H. Siegel, IEEE Trans. Microwave Theory Tech. **52**, 2438 (2004).
[3] D. Kindl, J. Touskova, E. Hulicius, J. Pangrac, T. Simecek, V. Jurka, P. Hubik, J. J. Mares, and J. Kristofik, J. Appl. Phys. **95**, 1811 (2004).
[4] Z. G. Hu, A. G. U. Perera, Y. Paltiel, A. Raizman, and A. Sher, J. Appl. Phys. **98**, 023511 (2005).
[5] M. Razeghi and H. Mosheni, in *Handbook of Infrared Detection Technologies*, edited by M. Henini and M. Razeghi (Elsevier, Amsterdam, 2002), Vol. 1, pp. 191–232.
[6] J. B. Rodriguez, P. Christol, F. Chevrier, and A. Joullie, Physica E (Amsterdam) **28**, 128 (2005).
[7] H. Mosheni, J. Wojkowski, M. Razeghi, G. Brown, and W. Mitchel, IEEE J. Quantum Electron. **35**, 1041 (1999).
[8] H. Mohseni, M. Razeghi, G. J. Brown, and Y. S. Park, Appl. Phys. Lett. **78**, 2107 (2001).
[9] D. G. Esaev, M. B. M. Rinzan, S. G. Matsik, A. G. U. Perera, H. C. Liu, B. N. Zvonkov, V. I. Gavrilenko, and A. A. Belyanin, J. Appl. Phys. **95**, 512 (2004).
[10] Y. Paltiel, A. Zussman, N. Snapi, A. Sher, G. Jung, K. Cohen, E. Benory, and E. Weiss, Infrared Phys. Technol. **47**, 37 (2005).
[11] W. Z. Shen and A. G. U. Perera, Infrared Phys. Technol. **39**, 329 (1998).
[12] K. Seeger, *Semiconductor Physics*, 9th ed. (Springer, Berlin, 2004), pp. 159–221, Chap. 6.
[13] D. G. Esaev, M. B. M. Rinzan, S. G. Matsik, and A. G. U. Perera, J. Appl. Phys. **96**, 4588 (2004).
[14] Y.-K. Su, Y.-Z. Chiou, F.-S. Juang, S.-J. Chang, and J.-K. Sheu, Jpn. J. Appl. Phys., Part 1 **40**, 2996 (2001).
[15] A. G. U. Perera, in *Homojunction and Quantum-Well Infrared Detectors*, edited by M. H. Francombe and J. L. Vossen (Academic, New York, 1995), Vol. 21, pp. 1–75.
[16] D. G. Esaev, S. G. Matsik, M. B. M. Rinzan, A. G. U. Perera, H. C. Liu, and M. Buchanan, J. Appl. Phys. **93**, 1879 (2003).